Research article

A Microfluidic Device for Spatiotemporal Delivery of Stimuli to Cells

Zubaidah Ningsih, James W.M. Chon and Andrew H.A. Clayton *

Centre for Microphotonics, Faculty of Science, Engineering and Technology, Swinburne University of Technology, John Street PO BOX 218 Hawthorn VIC 3122 Australia

* **Correspondence:** Email: aclayton@swin.edu.au; Tel: +61-3-9214-5719;
   Fax: +61-3-9214-5435.

Abstract: Living cells encounter many stimuli from the immediate environment. Receptors recognize these environmental cues and transduce signals to produce cell responses. The frequency of a signal is now emerging as an important factor determining cell responses. As a componentry system in understanding temporal stimulation, microfluidic devices allow the observation of cell behaviour under dynamic stimulation and controllable environment. In this paper we describe the design, construction and characterization of a microfluidic device suitable for cell stimulation studies.

1. Introduction

Living cells encounter many stimuli from the environment through cell-surface receptors which relay information to produce responses. Even though the signal transduction pathways share a common mechanism, in fact it is a very complex system that offers many possible kinds of cell response. Studies show that the qualitative and quantitative aspects of the signal are not the only factor determining signal transduction pathways [1,2]. The temporal aspect or frequency of a signal is now emerging as the other factor determining cell responses [3,4,5]. Kennedy et.al [6] successfully demonstrated the metabolic oscillation in β-cells and their interaction with extracellular Ca^{2+} changes. Modulation of Ca^{2+} concentration yields positive and negative feedback to the cell metabolism which is crucial in maintaining glucose homeostatis in blood.

Iqbal, et al. [7] attempted to review the hypothesis in explaining the complexity demonstrated by the modulation of signal amplitude and frequency. The delay between the stimulus reception and the cellular response is suspected to be the reason for complex cellular machinery. In this kinetic disconnect moment, a cell might undergo repetitive activation of numerous signaling pathways. In

addition, the kinase pathways inside the cell experience frequency and amplitude modulation. The authors argue that signal amplitude will determine the number of activated intracellular signaling molecules which influence the intensity of stimulus. In the meantime, intracellular signaling molecules could be translocated as a function of time and interact with a certain novel substrate in one time and another novel substrate at another time. Likewise, the inhibition of a certain signaling pathway by particular signaling molecules due to signal frequency modulation certainly will add to the complexity of cellular processes inside the cell. Thus, changing the signal frequency opens the doors for various possible ways of signaling pathways activation. Moreover, there is the uniqueness of multiple signal transduction pathways which are differentially controlled over time since this phenomenon would definitely impart specificity to cellular processes.

As a componentry system in understanding the cell system, microfluidics allow the observation of cells behaviour under dynamic stimulation and controllable environment [8]. Furthermore, fluid transport and delivery which occur within micrometre scale in diameter channels represents most biological application which makes microfluidics mimic what is happening in vivo [9]. Zhang et al. [10,11,12] attempted to produce microfluidic perfusion system for automated delivery of temporal gradients to Islets Langerhans. They included the internal pump and valve to control the stimulant gradient entering the system as well as altering the flow ratio to achieve necessary output concentration. To verify the output concentration and mixing, the authors applied fluorescein and detected its intensity as the parameter of stimuli gradient. Likewise, Schafer et.al [13] reported the fabrication of microfluidic and the mapping of chemical concentration in a microfluidic using two-photon absorption fluorescence imaging. Other perfusion system for cell study has been established by Cooksey et al. [14]. With 16 inlets, the system offers a multi-purpose microfluidic with combinatorial choice of inputs, mixtures, gradient patterns, and flow rates to accommodate temporal stimulation. Validation and verification of input-output concentration and mixing was performed using contrasting colour dye.

Despite the success of its fabrication, the aforementioned perfusion systems were verified using methods which unable to represent the detailed interaction of mixed species. In the first and second system, intensity was used to observe the output concentration which is susceptible to non-linearity in a dynamic condition. Similarly, the third system also used dye intensity which shares the same problem. Moreover, design complexity hinders an easy application.

On the other hand, FLIM (Frequency Lifetime Imaging Microscopy) was applied in several experiments to examine the distribution of mixed species [15,16]. Lifetime, which is the average amount of time a fluorophore remains in the excited state following excitation, overcomes the obstacle of intensity-based methods since it is independent of the number of fluorescing molecules [17]. Magennis et al. [18] compared intensity and lifetime images of 1,8-anilinonaphtalene sulfonate (ANS) in pure methanol and a water/methanol mixture. In intensity-based image, the distribution profile of ANS mixed with methanol showed irregular variations in intensity while the lifetime image presented a distinctive feature of species distribution. Mixing as a function of flow rate and flow distance has also been successfully demonstrated. Besides mixing extent, lifetime has also been applied to measure the concentration of the species mixed. Using NaI as the quencher of fluorescein, Robinson et al. [19] has demonstrated the quantitative mapping of a quencher concentration in three dimensions in a microfluidic device. The resulting experimental data was fitted to computational fluid-dynamics (CFD) simulation and showed good agreement.

Even though FLIM has shown robustness in qualitatively and quantitatively mapping the mixing inside microfluidic, this method has not been applied in observing spatiotemporal mixing inside microfluidic. Here, we demonstrate a simple PDMS microfluidic with adjustable frequency and amplitude. Using FLIM, our results exhibit a complete mixing between Rhodamine 6G and Potassium Iodide (KI) inside the microfluidic. Furthermore, a relationship between input-output KI concentrations based on its lifetime has exhibited the spatiotemporal delivery of the solutions. Cells were also successfully cultured inside the microfluidic.

2.   Materials and Method

2.1. Microfluidic fabrication

AutoCad 2013 was used to generate several 2D template designs which were printed on acetate mask with 20 μm resolution. The template of microfluidics was made from a photoresist chemical, SU-8 2015 (MMRC, Pty. Ltd.) on a surface of silicon wafer. The photoresist was coated on top of the silicon wafer through a spinner ramping with 1000 rpm velocity for 6 minutes. Then, the coated wafer was pre-baked at 95 °C for 5 minutes on a hot plate to complete the polymerization reaction. The UV light exposure energy applied was 150–160 mJ/cm^2 for 6 seconds. The coated wafer then post-baked at 95 °C for 5 minutes and followed by hard baked at 150 °C for 3 minutes. The photoresist then developed in developer solution and rinsed with IPA (isopropyl alcohol) where the non-exposed part of the coated silicon wafer will be washed away leaving the template design structure.

The fabrication of PDMS was conducted in the petri dish. Using scotch tape, the silicon wafer was securely positioned in the petri dish. The mixture of Slygard 184 silicon elastomer base and the curing agent (Dow Cowning) in 10:1 weight ratio then poured into the petri dish. To degas the bubble produced during the solution mixing, the petri dish was placed in the vacuum desicator. The petri-dish then placed in the oven at 60 °C overnight to let the PDMS cured. Using a scapel knife, the PDMS was cut out as the desired shape and removed from the wafer. The holes for the inlets were made by punching PDMS using biopsy punch. The PDMS then assembled with glass cover slip. Imprinted PDMS surface was bound to glass cover slip to produce sealed channels. PDMS and glass cover slip were placed in the plasma cleaner. The plasma cleaner then turned on for 50 s and a pale violet colour was present in the vacuum chamber during the process. After 50 s, the surface of glass cover slip and the imprinted PDMS were activated and ready for the binding. By pressing these two surfaces, PDMS and glass cover slip readily attach to each other. To enhance the binding, microfluidic was heated on hot plate at 75 °C for 5 minute.

2.2. Microfluidic characterization

The characterization step was aimed to confirm the channel structure produced and to examine the strength of PDMS and glass cover slip binding as well as the efficacy of solution mixing. 10 mM phosphate buffer (pH 7) or 300 mM KI in Milli-Q water were delivered through one inlet while the other inlet was set up to inject 10 μM^{-1} mM fluorescein, derived from fluorescein disodium salt solution in Milli-Q water, as the representative of stimuli. Solution filled syringes were mounted on PHD Ultra I/W Harvard programmable pump.

Furthermore, to establish relationship between input-output KI concentration for spatiotemporal mixing, 10 µM Rhodamine 6G were mixed with a mixture of 10 µM Rhodamine 6G and 100 mM KI. To achieve concentration modulation, a syringe filled with 10 µM Rhodamine 6G only solution was mounted to a programmable pump and set to have a ramp up and ramp down flow rate ranging from 0.1 to 1 µl/min. Similarly, the second syringe was filled with 10 µM Rhodamine 6G and 100 mM KI and mounted to the second programmable pump with the same range of flow rate. To have high concentration of KI, we set the flow rate of the second syringe ramped up from 0.1 to 1 µl/min. Meanwhile, the first syringe was set to have flow rate ramped down from 1 to 0.1 µl/min. And vice versa, the low concentration of KI was attained by ramping down the flow rate of second syringe from 1 to 0.1 µl/min and ramping up the first syringe from 0.1 µl/min to 1 µl/min. The characterization of microfluidic was performed using Fluorescence Lifetime Imaging Microscope (FLIM) with excitation from a 476 nm LED (Lambert Instruments, The Netherlands).

The analysis of images captured was performed using Li-FLIM software. The extent of mixing was determined by comparing the width of the channel occupied by fluorescein or Rhodamine 6G (marked by the fluorescence intensity and lifetime) compared to the total width of the channel. The measurement was conducted in the inlet channel and in the cell seeding area. By comparing between the fluorophore intensity and lifetime in the inlet channel and in the cell seeding area, the extent of the mixing can be calculated. The accuracy of KI concentrations delivered as a function of time was then confirmed by the comparison between the experimental results and the expected concentration based on the calculation.

2.3. Cell culture

HeLa cells were situated in 75 cm^2 tissue culture flask in Dulbecco's Modified Eagle Medium (DMEM; Sigma Aldrich, AU) containing 10% (v/v) foetal bovine serum (FBS; Life Technologies, AU), 1% (v/v) glutamine (Life Technologies, AU), 1% (v/v) penicillin/streptomycin (Life Technologies, AU) and 0.5% (v/v) amphotericin B (Life Technologies, AU). The culture was kept at 37 °C in a 95% humidified incubator with 5% CO$_2$. Prior to the use of cells in the experiment, the cells were passaged and maintained in culture for 3 days. Microfluidic was sterilized using UV light exposure for 30 minutes prior to the coating with 0.1 mg/ml Poly-D-lysine and was equilibrated using medium for overnight. Cells were then plated in microfluidic with cell density 4000–5000 cells/cm^2 and kept in the incubator for overnight to let the cells settle. The medium then continuously perfused from both arms with 0.08 µl/min flow rate for 8 hours and then stop the flow for the next 16 hours. The cycle was repeated for 7 days. The cell number changes were observed using bright field microscope on the daily basis.

3. Results
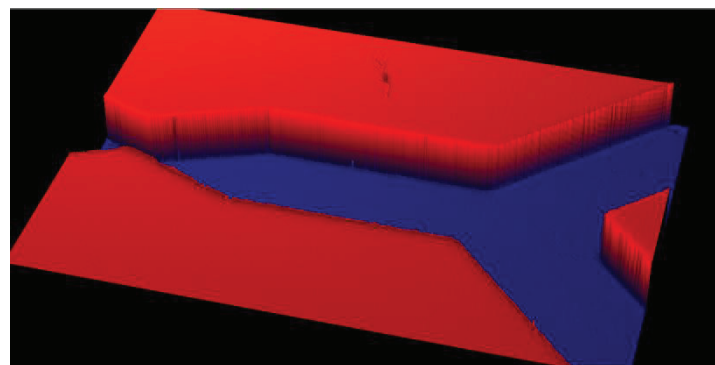
3.1. Microfluidic dimension

The microfluidic was designed with two arms. One arm is provided for the main stimulant while another arm is dedicated for the solvent to dilute the main stimulant. By varying the flow rate of solution from these two arms, the sinusoidal wave of stimulant concentration can be achieved. These
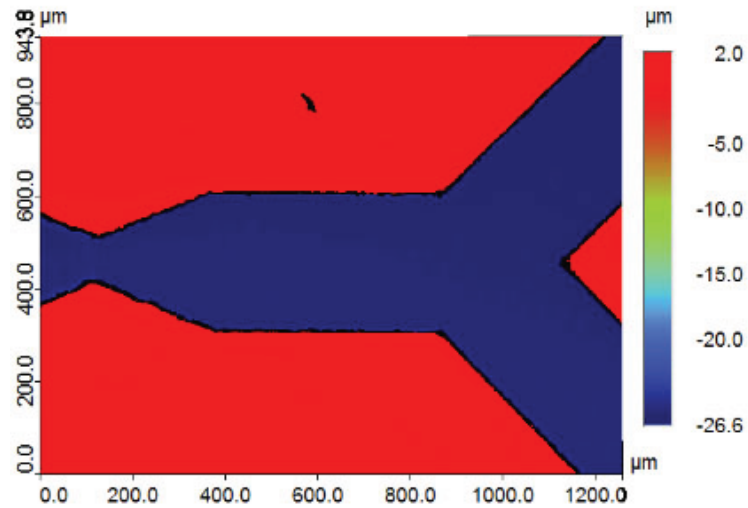
(a)

(b)

(c)

Figure 1. (a) Microfluidic channel, shown by dark region, has lower depth compared to the rest of PDMS surface. The average height of the channel was 25.32 μm (b) the measured width of the main channel was 296 μm (c) the 3D image of the channel imprinted on the surface of PDMS.

two arms then united in mixing area with various designs such as hurdles to perturb the flow and enhance the mixing. Between the mixing area and the outlet, the channel is designed as a straight channel for cell seeding area.

To confirm the dimension of the microfluidics, the imprinted channel on PDMS surface was coated using silver with 50 nm thickness using Magnetron Sputtering Physical Vapour Deposition technique. With 3D profiler, the height and the width of the channel were measured. Average height resulted from spinning at 1000 rpm for 6 minutes was 25.32 μm and the average width of the main channel was 296 μm (Figure 1). The length of the main channel of microfluidic was 3.16 cm. Since spinning speed at 1000 rpm in 60 second gave the closest height and width expected, which were 25 μm and 300 μm respectively, this setting was applied for all microfluidic designs.

3.2. Microfluidic flow characterization

Prior to the characterization of microfluidic, an experiment to confirm the linearity between the intensity and the concentration of fluorescein was conducted. The fluorescein concentrations applied were ranged from 0.1 μM–10 μM. In this characterization process, one inlet was filled with 10 μM fluorescein and the other inlet was loaded with 10 mM phosphate buffer (pH 7). For microfluidic design with 4 inlets, 2 inlets were filled with fluorescein and the rest were loaded with buffer. The images captured then converted to intensity profile as a function of Y position. The intensity profile plot was drawn from the average of 12 vertical lines at a certain Y position. Each line represents the intensity along particular Y position. From this plot, description of the area in the channel occupied by the fluorescein can be drawn. The graph showing the linearity between fluorescein intensity and concentration together with the illustration of the image conversion is presented in Figure 2.

Intensity distribution in the beginning of inlets junction was compared to the intensity distribution in the cell seeding area to quantify the extent of mixing. The distribution of intensity was determined via the width of the peak which represents the width of channel filled with fluorescein. The percentage of channels area loaded by fluorescein was derived from the comparison between the width of the channel filled with fluorescein and the total width of the channel.

From the comparison of several designs, hurdle design gave the most satisfactory result. In mixing part, the width of the channel was designed to narrow down from 300 μm to 50 μm to create hurdle for the flow. The width reduction was repeated up to 10 times. In this design the cell seeding area filled with fluorescein was up to 86%. Further analysis shows that the intensity distribution in this design was increasing from 61% in the inlets junction, 63% in the first unit of hurdle, 79% in the second hurdle unit, 83% in the last hurdle unit and 86% in cell seeding area (Figure 3). Based on these results, the hurdle design gives a satisfactory mixing extent compared to the other designs.
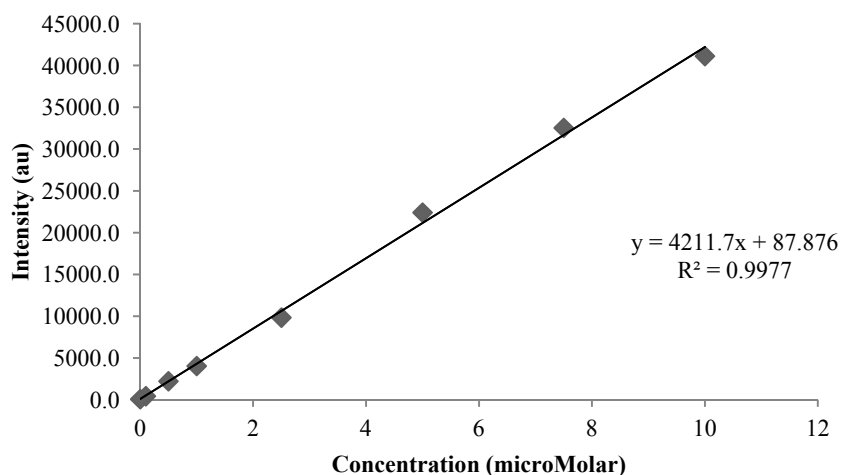
(a)
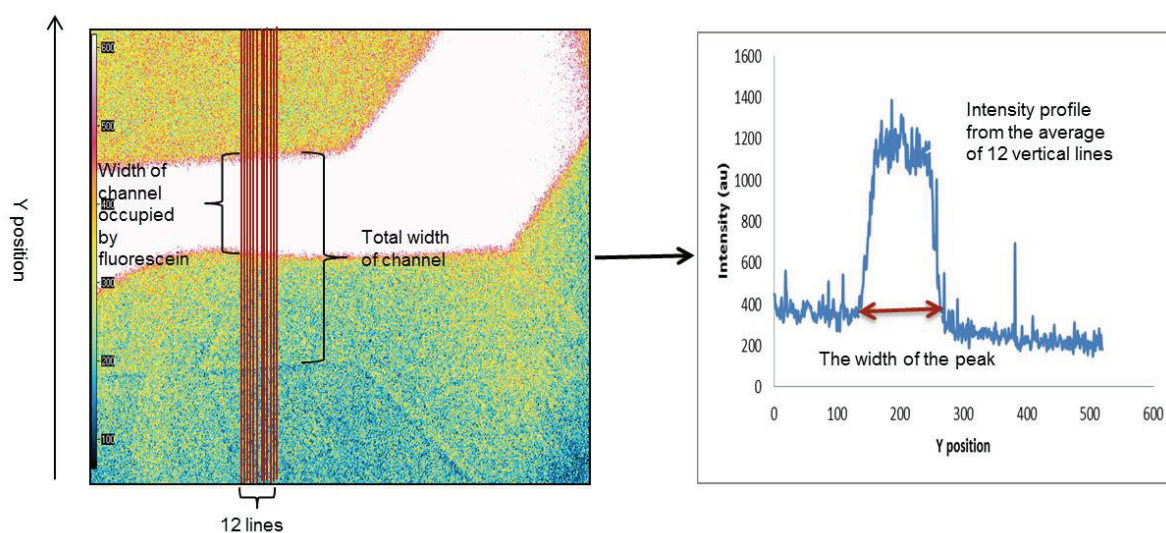
(b)

Figure 2. (a) The graph shows the linearity of fluorescein intensity as a function of concentration. (b) The illustration of image to intensity graph conversions as a function of Y position.

To confirm the solution mixing, fluorescein intensity measurement in the presence of 300 mM KI was performed. KI act as the quencher which reduces the intensity of fluorescein whenever the two solutions mixed. In this experiment, one inlet was filled with fluorescein while the other inlet was loaded with buffer or 300 mM KI as the quencher. As shown in Figure 4, area occupied by fluorescein was narrow at the beginning and began to expand as the distance from the inlet junction increased. Reaching cell seeding area, the intensity decreased and it was detected throughout the channel. The distinct high and low fluorescein intensity area was diminishing which substantiate the quenching of KI as it mixed with fluorescein (Figure 4).
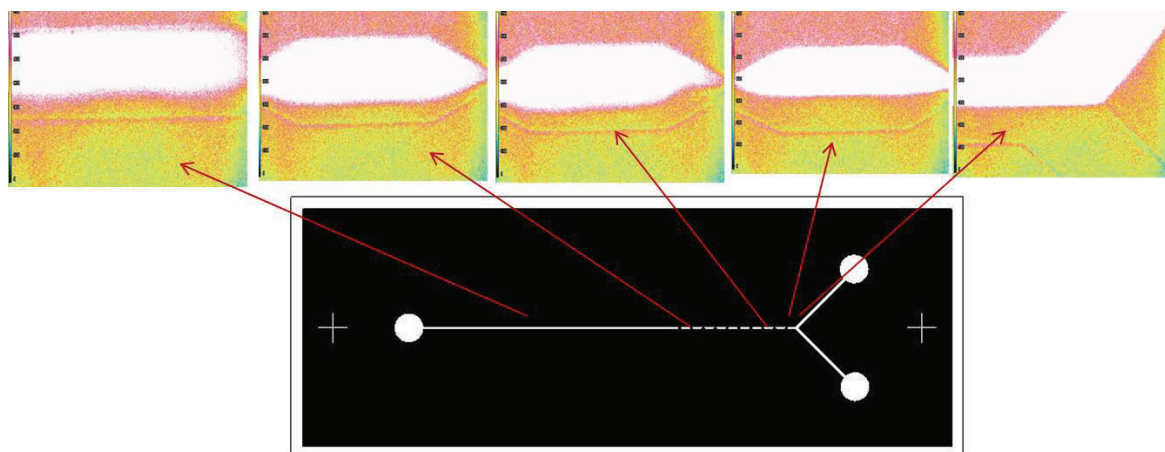
Figure 3. The structure of hurdle design pattern. The inserted images on top of the design are the fluorescein intensity images from the inlet up to the cell seeding area. The increasing bright area from the inlet junction to the cell seeding area substantiates the mixing of fluorescein and buffer.
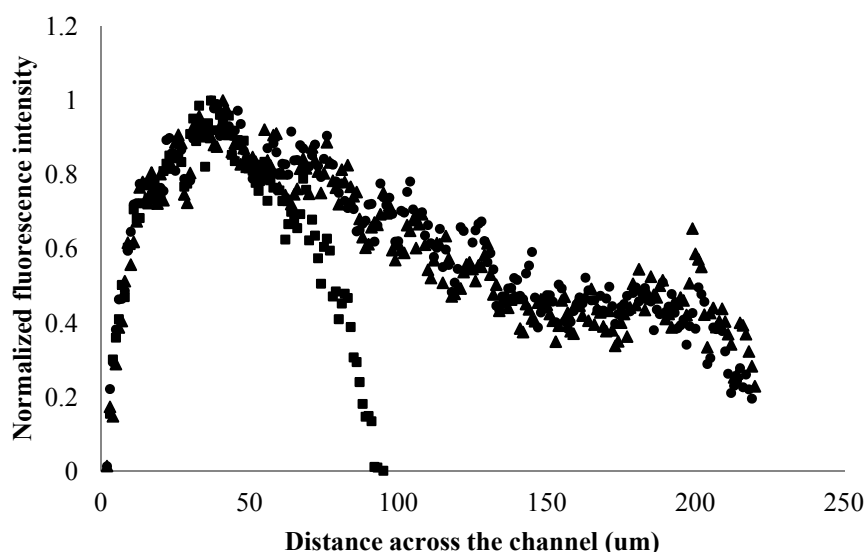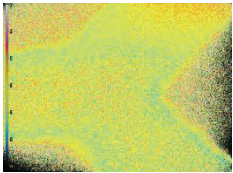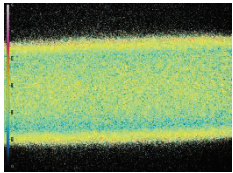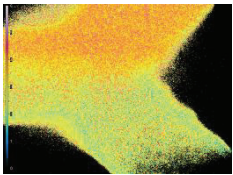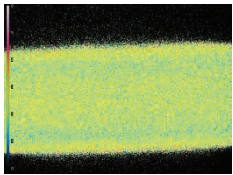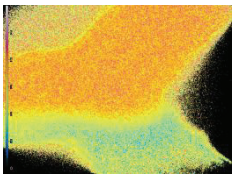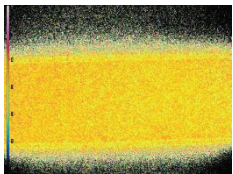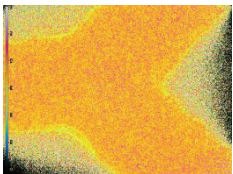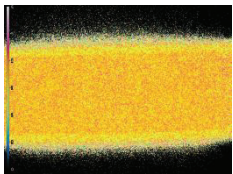

Figure 4. Filled square structure represents fluorescein intensity at the beginning of the channel. The intensity was noticeable only up to half of the channel area. Further along the channel, the intensity decreases (represent by the triangle and circle structure). The broaden graph signifies the increase of area occupied by fluorescein due to the mixing of fluorescein and KI.

Even though mixing has been demonstrated, there is a considerable variation in fluorescence intensity indicated by the non-linear intensity value detected in the cell seeding area. To have a more accurate observation of mixing extent, we utilize lifetime as the parameter. Lifetime has been shown to offer a reliable result in imaging inside microfluidic [19]. As described in method section, two

filled syringes were mounted to programmable pumps which enable the delivery of modulated flow. First syringe filled with 10 µM Rhodamine 6G and the second syringe filled with a mixture of 10 µM Rhodamine 6G and 100 mM KI. Table 1 shows the comparison between the average lifetime measured in the inlet and the cell seeding area as a function of flow rate.

Table 1. The average lifetime in inlet and cell seeding area as a function of flow rate.

Flow rate of 10 µM Rhodamine 6G (µl/min)	Flow rate of 10 µM Rhodamine 6G and 100 mM KI (µl/min)	Image in inlet area	Average lifetime in inlet (ns)	Image in cell seeding area	Average lifetime in cell seeding area (ns)
0.25	0.75		2.79 ± 0.84		1.97 ± 0.75
0.5	0.5		3.25 ± 0.77		2.01 ± 0.58
0.75	0.25		3.32 ± 0.69		2.80 ± 0.55
1	0.1		3.73 ± 0.47		3.55 ± 0.56

Further along the channel, it can be seen that the mixing extent between two solutions is increasing. Distinguishable area between fast and slow lifetime in inlet is gradually diminishes and reaches homogeneity in cell seeding area. Changes in lifetime also signify the mixing due to KI quenching. Furthermore, the average lifetime in cell seeding area descending as the KI flow rate ascending and vice versa. Thus, varying flow rate produces lifetime modulation which signifies sinusoidal wave of KI.

To further analyze the results, lifetime distribution in inlet was compared to the lifetime distribution in cell seeding area. Figure 5 represents the comparison of lifetime distribution at equal flow rate between 2 syringes. Dashed line exhibits lifetime distribution across the channel in inlet while the continuous line represents the lifetime distribution in cell seeding area. In the left side of the channel which filled with 10 µM Rhodamine 6G, the lifetime is longer compared to the right side

that contained 10 µM Rhodamine 6G and 100 mM KI. This indicates that at the beginning of the solutions encounter, KI has not yet mixed homogenously. As the solutions move along the channel, more mixing took place shown by the decrease of lifetime with more homogenous distribution in cell seeding area. The previously longer lifetime species is quenched by KI which disperses to wider area in the channel. It denotes the complete mixing inside the microfluidic channel.
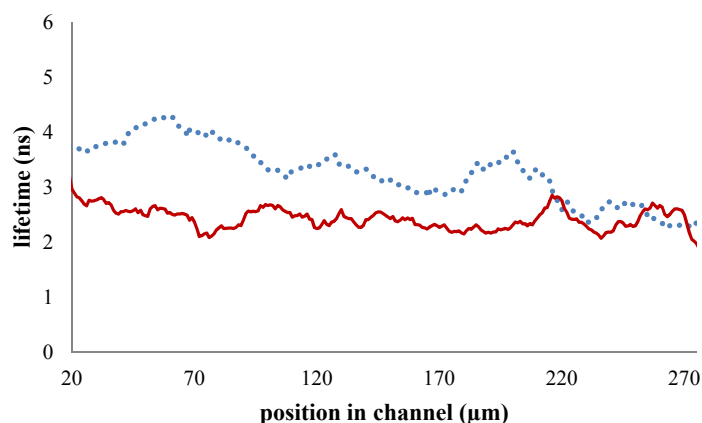

Figure 5. Comparison between lifetime distribution in inlet (dashed line) and cell seeding area (continuous line). The data shown is a moving average of every 20 pixels. Mixing is marked by the decrease of Rhodamine 6G lifetimes due to being quenched by KI. More homogeneous distribution in cell seeding area represents the complete mixing inside microfluidic channel.
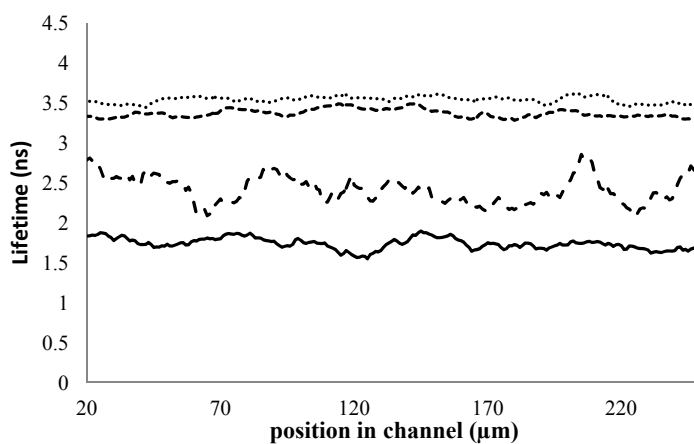

Figure 6. Comparison of lifetime distribution in cell seeding area as a function of KI flow rate. Dotted line (0.1 µL/min), dashed small line (0.25 µL/min), dashed large line (0.5 µL/min), and continuous line (0.75 µL/min).

Comparison of lifetime distribution in cell seeding area as a function of KI solution flow rate is shown in Figure 6. When a mixture of 10 µM Rhodamine 6G and 100 mM KI solutions flow faster than 10 µM Rhodamine 6G solution, the lifetime is shorter due to the quenching which indicates the

high concentration of KI present. Vice versa, when the flow of solution containing KI is slow, lifetime value increases which point out the low concentration of KI.

Furthermore, by ramping up and down the flow rate of two solutions for 140 minutes, we generate a sinusoidal pattern of Rhodamine 6G lifetimes for spatiotemporal delivery (Figure 7a). In the first 30 minutes lifetime is increasing which indicate KI concentration reduction. For the next 30 minutes KI concentration started to increase which causes the decrease in Rhodamine 6G lifetime. This pattern was then repeated for the next 60 minutes which produced a spatiotemporal delivery. Using Stern-Volmer plot, fluorescein lifetime (in the presence of KI) was then converted to concentration (Figure 7b). The plot characterizes input-output relationship of KI concentration with specific amplitude, frequency and phase. The KI concentration measured has a similar pattern with the predicted concentration based on calculation. These results demonstrate that the frequency, amplitude and phase of the input and output concentration can be regulated as needed.
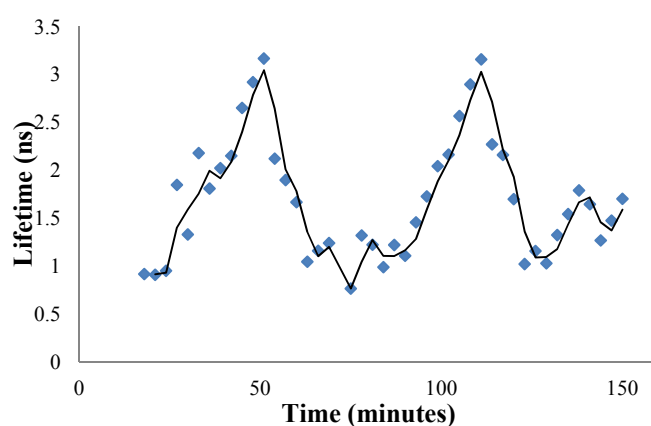
(a)
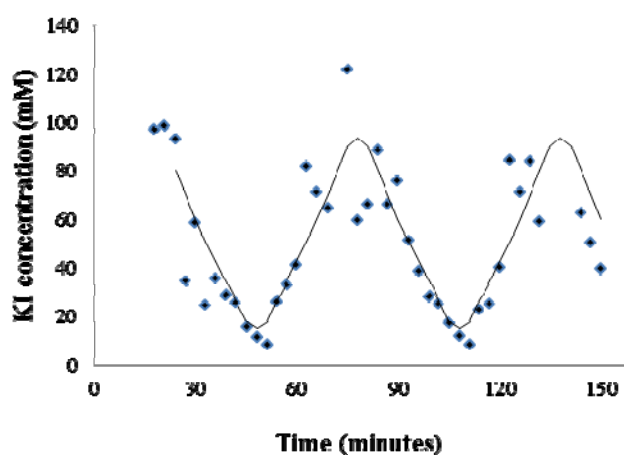
(b)

Figure 7. Rhodamine 6G lifetime in the presence of KI oscillates as the flow rate of KI was modulated (a). The continuous line is moving average of 2 data points as a guide to see the pattern. Plot of KI concentration shows the sinusoidal wave with frequency 60 minutes per cycle and 0–100 mM amplitude (b). The continuous line represents the calculated KI concentration.

3.3. Cell culture inside microfluidic

To characterize the biocompatibility of the microfluidic device produced, HeLa cells were cultured inside microfluidic. Proliferation was observed via increases in cell number with time. We have observed cell viability in several flow rates in certain duration. The flow rates applied were 0.25; 0.15; 0.1 and 0.08 µl/min. At high flow rate cells tended to detach in less than 24 hours perfusion. Meanwhile, cells remain attached and proliferated when we applied 0.08 µl/min flow rate for 8 hours and then stop the flow for the next 16 hours and repeat the cycle for 7 days. Hung et.al [20] observed that HeLa cells cultured under 0.12 µl/min perfusion of medium grew exponentially after 3 days. In our system, cell number was constant until day 5 and then increased rapidly up to 500% at day 8 (Figure 9). Cell viability was marked with the spreading and the outgrowth of the cell on the microfluidic surface in the entire course of study.

day 1   day 5   day 6
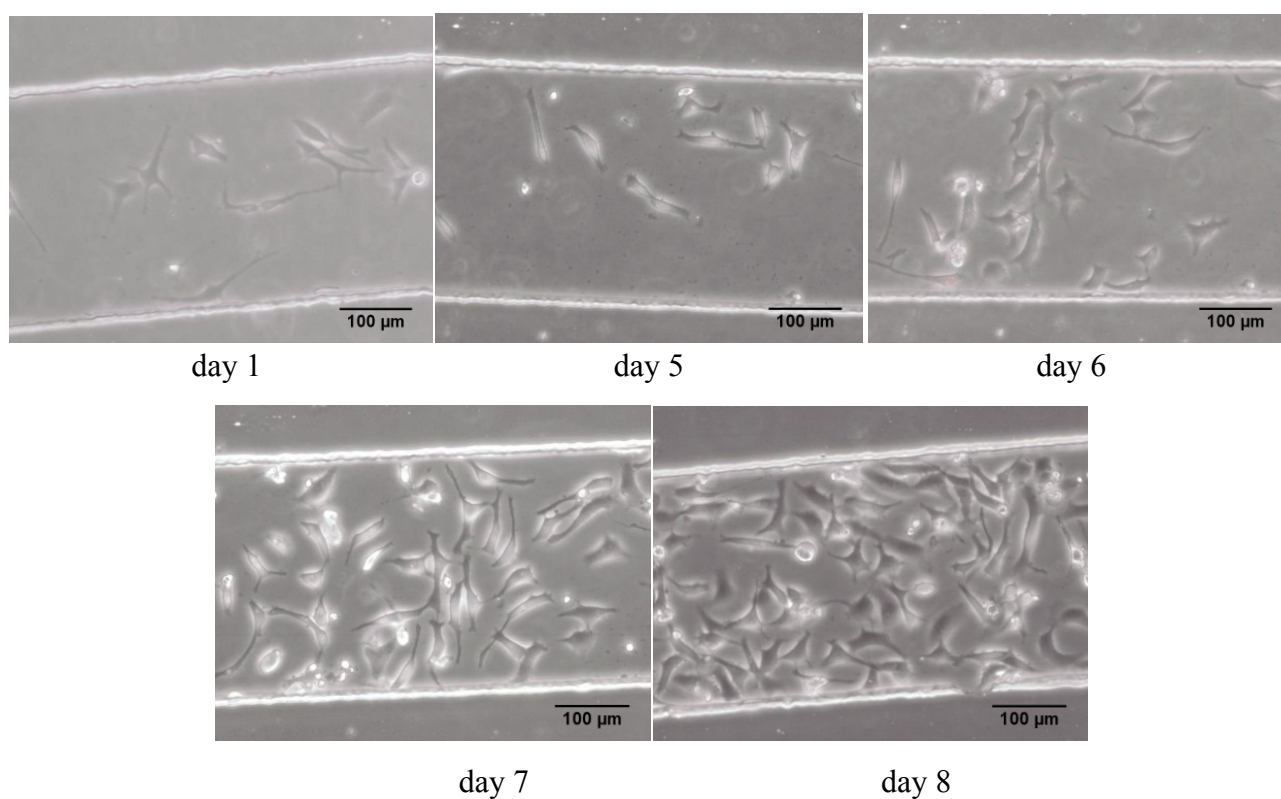
day 7   day 8

Figure 8. HeLa cells showed cell attachment to the base of microfluidic after 1 day incubation followed with rapid proliferation after day 5 under perfusion of medium with 0.08 μl/min flow rate.
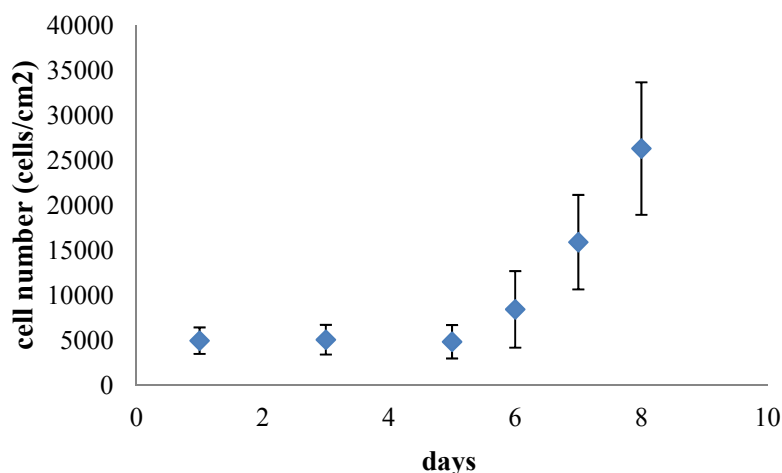
Figure 9. Cell number as a function of time shows that the cells start to proliferate after day 5 and increase rapidly up to 500% at day 8.

4. Discussion

The images of fluorescein intensity in hurdle design along the microfluidic channels show that the perturbation of laminar flow indeed succeeded to increase the mixing of two solutions. The hurdles produce pressure which disturbs the laminar flow to facilitate mixing. This is confirmed by further experiment using KI as the quencher. Figure 3 shows the broadening of fluorescein intensity which substantiate the fluorophore diffusion throughout the channel. The decrease of intensity also signifies the reduction of fluorescein concentration at the downstream of fluorescein inlet since it disperses to wider area. Figure 4 confirms the mixing where fluorescein is being quenched by KI. The intensity at the downstream of KI inlet was shorter than at fluorescein downstream which denotes the encounter of fluorescein and KI.

Even though mixing was observed, hurdle design was unable to produce a complete mixing. In equilibrium, there was region along the channel in cell seeding area where fluorescein was not detected. To overcome this problem, we use a straight channel with slower solution flow rate. Magennis et al. [18] has demonstrated that mixing extent has a reverse relationship with flow rate. The slower the flow rate, the more mixing occurs. Furthermore, instead of observing the intensity, lifetime was used as the observation parameter. Figure 4 and 5 demonstrate the difference between intensity and lifetime observation. In Figure 5, even though the spreading of the solution was detected, fluorescein intensity observed in equilibrium was not linear. High intensity was detected at the downstream of fluorescein inlet and decreasing at further distance. This result is in agreement with Magennis et al. [18] that discovers a considerable variation in fluorescence intensity during the mixing due to optical artifacts. On the other hand, Figure 5 shows a constant Rhodamine 6G lifetime in cell seeding area which represents solely the environment of the fluorophore. Hence, lifetime is a robust parameter to characterize the mixing inside microfluidic.

As mentioned above, the flow rate was reduced to 0.1–1 μl/min to increase the mixing extent. Moreover, different flow rate between two inlets was applied to achieve concentration modulation. Rhodamine 6G lifetime in the presence of different KI concentration was monitored to detect mixing

extent and concentration modulation. Table 1 summarizes the comparison between lifetime in inlet and in cell seeding area. The average lifetime in cell seeding area is linear with KI flow rate. Fast KI flow rate produces shorter lifetime, and vice versa slow KI flow rate yields longer lifetime. The average lifetime in inlet decreased from 2.79 ± 0.84–3.73 ± 0.47 to 1.94 ± 0.89–3.55 ± 0.56 ns. The decrease substantiates the diminishing of longer lifetime species in inlet due to KI quenching as they are mixed. To confirm the complete mixing, profiles of lifetime distribution in cell seeding area as a function of KI flow rate were drawn as shown in Figure 6. Lifetime distributions are relatively uniform throughout the channel. It also shows the linear trend where faster KI flow rate produces shorter lifetime.

Our results also demonstrate the sinusoidal wave of KI concentration. By ramping up the flow rate of 10 µM Rhodamine 6G and 100 mM KI and simultaneously ramping down the flow of 10 µM Rhodamine 6G, high amplitude was achieved. Low amplitude was performed when the flow rate of 10 µM Rhodamine 6G and 100 mM KI was ramping down while the flow rate of 10 µM Rhodamine 6G was increasing. By changing the flow rate of two solutions, there is control of KI concentration delivery as a function of time. From our result, the measured KI shows an agreement with the calculated KI concentration.

Cell culturing inside microfluidic exhibited satisfactory results where cells were successfully shown to proliferate. At high flow rate of medium, cells remained attached during a short period of stimuli perfusion while decreasing the flow rate improved cell viability for a longer period of perfusion. These results show that microfluidic produced have a suitable dimension and biocompatibility for cell growth under transient perfusion of stimuli.

5.   Conclusion

Our results demonstrate that complete mixing inside microfluidic was achieved. By varying the flow rate between inputs, KI concentration modulation with adjustable amplitude, frequency and phase was successfully established. Cells were successfully cultured inside the microfluidic. This signifies that the system is a suitable device for spatiotemporal delivery in cell signaling studies.

Acknowledgments

Conflict of Interest

All authors declare no conflicts of interest in this paper.

References

1. Behar M, Hao N, Dohlman HG, et al. (2008) Dose to duration encoding and signaling beyond saturation in intracellular signaling networks. *PLoS Computat Biol* 4: 1–11.
2. Brent R (2009) Cell signaling : What is the signal and what information does it carry? *Federation

of European Biochemical Societies 583: 4019–4024.

3. Cai L, Dalal CK, Elowitz MB (2008) Frequency-modulated nuclear localization bursts coordinate gene regulation. *Nature* 455: 485–491.

4. Domletsch RE, Xu K, Lewis RS (1998) Calcium oscillations increase the efficiency and specificity of gene expression. *Nature* 392: 933–936.

5. Zhu X, Si G, Deng N, et al. (2012) Frequency-dependent Escherichia coli chemotaxis behavior. *Phys Rev Lett* 108: 128101.

6. Kennedy RT, Kauri LM, Dahlgren GM, et al. (2002) Metabolic oscillations in β-cells. *Diabetes* 51: S152–S161.

7. Iqbal J, Li S, Zaidi M (2010) Complexity in signal transduction. *Ann N Y Acad Sci* 1192: 238–244.

8. Godin J, Chen C-H, Cho SH, et al. (2008) Microfluidic and photonics for Bio-System-an-a-chip : A review of advancements in technology towards a microfluidic flow cytometry chip. *J Biophotonics* 5: 355–376.

9. Mampallil D, George DS (2012) Microfluidics- A lab in your palm. *Resonance* 682–690.

10. Zhang X, Roper MG (2009) Microfluidic perfusion system for automated delivery of temporal gradients to Islets of Langerhans. *Anal Chem* 81: 1162–1168.

11. Zhang X, Grimley A, Bertram R et al. (2010) Microfluidic system for generation of sinusoidal glucose waveforms for entrainment of Islets Langerhans. *Anal Chem* 82: 6704–6711.

12. Zhang X, Dhumpa R, Roper MG et al. (2013) Maintaining stimulant waveforms in large-volume microfluidic cell chambers. *Microfluid Nanofluid* 15: 65–71.

13. Schafer D, Gibson EA, Amir W, et al. (2007) Three-dimensional chemical concentration maps in a microfluidic device using two-photon absorption fluorescence imaging. *Opt Lett* 32: 2568–2570.

14. Cooksey GA, Sip CG, Folch A (2009) A multi-purpose microfluidic perfusion system with combinatorial choice of inputs, mixtures, gradient patterns, and flow rates. *Lab Chip* 9: 417–426.

15. Elder AD, Mattews SM, Swartling J, et al. (2006) The application of frequency-domain Fluorescence Lifetime Imaging Microscopy as a quantitative analytical tool for microfluidic devices. *Opt Express* 14.

16. Zeng Y, Jiang L, Zheng W, et al. (2011) Quantitative imaging of mixing dynamics in microfluidic droplets using two-photon fluorescence lifetime imaging. *Opt Lett* 36: 2236–2238.

17. Lakowitz JR (2006) Principles of Fluorescence Spectroscopy, 3rd ed., New York: Springer Science+Business Media, LLC.

18. Magennis SW, Graham EM, Jones AC (2005) Quantitative spatial mapping of mixing in microfludic system. *Angewandte Chemie International Edition* 44: 6512–6516.

19. Robinson T, Valluri P, Manning HB, et al. (2008) Three-dimensional molecular mapping in a microfluidic device using fluorescence lifetime imaging. *Opt Lett* 33: 1887–1889.

20. Hung PJ, Lee PJ, Sabounchi P, et al. (2005) Continuous perfusion microfluidic cell culture array for high-throughput cell-based assays. *Biotechnol Bioeng* 89: 1–8.